International Journal of Biological Macromolecules 356 (2026) 151590

Contents lists available at ScienceDirect

International Journal of Biological Macromolecules

journal homepage: www.elsevier.com/locate/ijbiomac

Bioprocess engineering as a tool to modulate the rheological performance of *Ensifer meliloti* SEMIA 135 exopolysaccharide

Rui dos Santos Ferreira Filho [a,*], Filomena Freitas [b,c], Janaína Fernandes de Medeiros Burkert [a], Carlos André Veiga Burkert [a]

[a] Bioprocess Engineering Laboratory, School of Chemistry and Food, Federal University of Rio Grande, 96203-900, Rio Grande, RS, Brazil
[b] UCIBIO — Applied Molecular Biosciences Unit, Department of Chemistry, School of Science and Technology, NOVA University Lisbon, 2829–516, Caparica, Portugal
[c] i4HB — Institute for Health and Bioeconomy, School of Science and Technology, NOVA University Lisbon, 2829-516, Caparica, Portugal

ARTICLE INFO

Keywords:
Biopolymers
Bioreactor hydrodynamics
Diazotrophic bacteria
Gelation
Thixotropy
Viscoelasticity

ABSTRACT

The controlled production of microbial polysaccharides offers a powerful route to design renewable materials with tailored functionalities. In this work, the influence of bioreactor hydrodynamics on the structure and macroscopic properties of the exopolysaccharide produced by *Ensifer meliloti* SEMIA 135 was systematically investigated. Aeration (0.8–2.2 vvm) and agitation (59–341 rpm) were varied according to a Central Composite Rotatable Design, revealing a strong interaction effect on polymer composition and viscosity. Variations in cultivation conditions modulated the apparent viscosity from 68.7 to 228.3 Pa·s, correlated with a variation in total uronic acid content from 2.91% to 11.96%, confirming the key role of charge density in defining molecular organization. The polymer formed weak, pseudoplastic, and thixotropic gels, with the storage modulus (G') consistently higher than the loss modulus (G'') across all frequencies. Its viscoelastic profile was highly dependent on concentration (0.01–3.0 wt%), pH (3–9), and temperature, showing a sol–gel transition near 70 °C and enhanced elasticity at acidic and alkaline pH. Deviations from the Cox–Merz rule indicated the presence of a structured associative network rather than a simple entangled solution. Overall, this study demonstrates that fine-tuning of cultivation conditions can be used as a predictive tool to control the molecular architecture and rheological performance of bacterial polysaccharides, establishing a rational bioprocessing framework for the development of functional biomaterials.

1. Introduction

The global demand for hydrocolloids with specific, predictable rheological behaviors is rising, driven by their widespread application in food [1,2], cosmetic, pharmaceutical, and biomedical formulations [3–5], as these polymers are essential for controlling texture, stability, and processability. Concurrently, a market-driven search for renewable and biodegradable alternatives to synthetic polymers has intensified the focus on microbial biopolymers [6]. Among these, microbial exopolysaccharides (EPS) have attracted significant attention due to their structural versatility, biocompatibility, and the potential to modulate their properties through bioprocess engineering [7].

EPS are high-molecular-weight polymers secreted by bacteria, yeasts, and fungi. Their complex chemical architecture, often comprising diverse neutral sugars, amino sugars, and uronic acids, results in sophisticated rheological behaviors that define their functional potential [8,9]. The key advantage of microbial EPS over plant- or algal-derived counterparts lies in their production: they can be synthesized in controlled bioreactors, offering a unique pathway to tune their final composition. This 'bio-factory' approach presents an opportunity to rationally design rheology modifiers with tailored performance [10,11].

Despite this potential, a persistent gap exists in the literature: a systematic understanding of how upstream bioprocess conditions influence the final molecular structure and properties of these polymers [12,13]. Most research has traditionally been siloed, focusing either solely on optimizing cultivation yield or on characterizing the rheology of obtained polymers, rarely establishing the critical quantitative link between the bioreactor environment and the material's functionality. This disconnection between bioprocesses, structure, and function prevents the rational design of EPSs with predetermined characteristics and constrains their broader industrial adoption [13].

Among the various process parameters, aeration and agitation were

* Corresponding author.
E-mail address: ruiferreirafilho@outlook.com (R.S. Ferreira Filho).

https://doi.org/10.1016/j.ijbiomac.2026.151590
Received 12 November 2025; Received in revised form 11 March 2026; Accepted 20 March 2026
Available online 21 March 2026

selected as the primary factors for this investigation because they fundamentally define the physical and physiological environment in stirred-tank bioreactors [14]. Together, they govern the oxygen transfer rate (OTR) and the hydrodynamic shear stress, which are known to exert opposing effects on polymer quality. On the one hand, oxygen availability dictates the energy metabolism (ATP generation) required for the synthesis of activated nucleotide sugar precursors (e.g., UDP-glucose, UDP-glucuronic acid), directly influencing the monosaccharide composition and charge density of the EPS [7,15,16]. On the other hand, the shear stress generated by agitation affects the physical integrity of the polymer; excessive shear can cause macromolecular degradation, reducing molecular weight and, consequently, diminishing the pseudoplastic and thixotropic behavior of the broth [17,18]. Conversely, insufficient mixing leads to heterogeneity and oxygen limitation, which may trigger metabolic shifts favoring the incorporation of specific monomers [19].

Therefore, changes in bioreactor hydrodynamics can cause significant variations in the monosaccharide composition, charge density, and molecular weight distribution of the resulting EPS. These structural changes are the direct drivers of rheological performance: for instance, a higher molecular weight or increased uronic acid content typically enhances chain entanglement and electrostatic repulsion, leading to higher viscosity, stronger shear-thinning (pseudoplastic) behavior, and distinct time-dependent (thixotropic) recovery [20,21]. Quantifying this relationship is essential to transform cultivation from a trial-and-error process into a predictable tool for materials design.

This study directly addresses this gap by validating the use of controlled bioprocess conditions to engineer the rheological properties of EPS. Therefore, the specific objectives of this work were: (i) to systematically evaluate the interactive effects of aeration and agitation on the monosaccharide composition and charge density of *E. meliloti* SEMIA 135 EPS using a Central Composite Rotatable Design (CCRD); (ii) to establish direct quantitative correlations between the bioprocess variables, the polymer's chemical composition, and its final macroscopic viscoelastic response; and (iii) to comprehensively characterize the physical stability and thixotropic behavior of the polymer under varying pH, concentration, and temperature conditions. By addressing these objectives, this work establishes a quantitative framework connecting cultivation hydrodynamics to the final material functionality, demonstrating a scalable strategy for producing biopolymers with targeted rheological profiles.

2. Materials and methods

2.1. Exopolysaccharide production and purification

The EPS was produced by the bacterium *Ensifer meliloti* SEMIA 135, provided by the SEMIA Rhizobia Collection (DDPA, RS, Brazil). Stock cultures were maintained on yeast mannitol agar (YMA) at 4 °C. The inoculum was prepared by suspending cells in 0.1% (*w/v*) peptone (Kasvi, Curitiba, PR, Brazil) diluent and transferring them to 500 mL Erlenmeyer flasks containing 90 mL of YMA broth (pH 7.0). The flasks were incubated in an orbital shaker (TE-420, Tecnal, Piracicaba, SP, Brazil) at 30 °C and 200 rpm until an optical density (OD) of 0.8 was reached at 600 nm.

Cultivations were performed in a 5 L stirred-tank bioreactor (Biostat B, B. Braun Biotech International, Melsungen, Germany) with a working volume of 4 L (10% *v*/v inoculum). The temperature was maintained at 30 °C, and the pH was not controlled during the process. The culture medium contained soybean molasses (CJ Selecta, Araguari, MG, Brazil) (30 g L^{-1}) as the primary carbon and nitrogen source, supplemented with (g L^{-1}): K_2HPO_4 (0.1), $MgSO_4{\cdot}7H_2O$ (0.2), and $CaCl_2{\cdot}2H_2O$ (0.15) (all from Synth, Diadema, SP, Brazil); KH_2PO_4 (0.4) and NaCl (0.1) (Dinâmica, Indaiatuba, SP, Brazil); and $MnCl_2{\cdot}7H_2O$ (0.12) (Vetec, Duque de Caxias, RJ, Brazil), according to Ferreira Filho et al. [22].

To investigate the impact of production parameters on the final polymer characteristics, distinct samples were obtained following a 2^2 Central Composite Rotatable Design (CCRD) with three central points. The independent variables (factors) were aeration, ranging from 0.8 to 2.2 vvm, and agitation, ranging from 59 to 341 rpm. These ranges were selected to expand upon the baseline conditions previously established for this strain (1.25 vvm and 100–200 rpm) [22], aiming to capture a broader spectrum of hydrodynamic stress and evaluate its consequential impact on the macroscopic properties of the polymer. This design resulted in 11 experimental runs, which yielded the EPS samples subsequently used for chemical and rheological characterization.

After cultivation, the culture broth was centrifuged (13,000 ×*g*, 30 min, 4 °C) to remove the bacterial cells. The EPS was then precipitated from the cell-free supernatant by adding three volumes of cold 96% ethanol (Hyplass, São Paulo, SP, Brazil). For the characterization studies, the recovered EPS was redissolved in MilliQ water (Millipore, Burlington, MA, USA) and purified by dialysis against deionized water using cellulose membranes (12 kDa molecular weight cutoff, Inlab, Diadema, SP, Brazil) for 72 h, with water changes every 24 h, to ensure the removal of salts and residual low-molecular-weight compounds (including free sugars from the culture medium), retaining only the high-molecular-weight biopolymer fraction [22]. Finally, the samples were lyophilized to obtain a purified, dry powder for analysis.

2.2. Exopolysaccharide carbohydrate composition

For identification and quantification of the monosaccharide composition, the 11 EPS samples obtained from the CCRD were subjected to acid hydrolysis. Briefly, the samples were hydrolyzed using 2 M trifluoroacetic acid (TFA) (Sigma-Aldrich, Darmstadt, Germany; 99.0%) at 120 °C for 1 h in hermetically sealed tubes to minimize oxygen exposure. The resulting hydrolysates were then analyzed by high-performance anion exchange chromatography with pulsed amperometric detection (HPAEC-PAD). The HPAEC-PAD analysis was performed following the methodology described by Concórdio-Reis et al. [8]. Briefly, a Dionex ICS-6000 system (Thermo Scientific Dionex, Sunnyvale, CA, USA) equipped with a Dionex CarboPac PA100 analytical column (250 mm × 4 mm) maintained at 30 °C was used. Detection was carried out by an electrochemical detector in integrated amperometry mode. The separation was conducted at a 1 mL min^{-1} flow rate with an injection volume of 25 μL using a gradient elution composed of Milli-Q water (A), 500 mM NaOH (B), and 500 mM sodium acetate (C). Calibration curves were prepared in the 5 to 100 μg mL^{-1} range using the following standards: fucose (Biosynth, Staad, Switzerland; 98.0%), rhamnose (Fluka, Buchs, Switzerland; 99.0%), arabinose (TCI, Tokyo, Japan; 98.0%), glucosamine (TCI, Tokyo, Japan; 98.0%), galactose (Thermo Fisher Scientific, Waltham, MA, USA; 98.0%), glucose (Fisher Scientific, Hampton, NH, USA; 99.0%), mannose (Sigma–Aldrich, St. Louis, MO, USA; 99.0%), ribose (Sigma–Aldrich, St. Louis, MO, USA; 98.0%), galacturonic acid (Sigma–Aldrich, St. Louis, MO, USA; 97.0%), and glucuronic acid (Thermo Fisher Scientific, Waltham, MA, USA; 98.0%).

2.3. Rheological characterization

The rheological properties of the EPS solutions were investigated under various conditions of shear, temperature, and time. For the 11 samples obtained from the experimental design, the apparent viscosity at a shear rate of 0.01 s^{-1} was selected as the key response variable for statistical analysis. The experimental data were used to develop a predictive model using Statistica software (v. 12.0, StatSoft, Inc., Tulsa, OK, USA). The statistical significance of the model was evaluated by analysis of variance (ANOVA), and a contour plot was generated to visualize the relationship between the production variables and the resulting apparent viscosity.

Table 1
Central Composite Rotatable Design (CCRD) matrix with coded (real) values and the corresponding viscosity and monosaccharide composition responses of the EPS samples.

Sample	X_1	X_2	Viscosity (Pa·s)	Composition (%)									
	Aeration (vvm)	Agitation (rpm)		Fuc	Rha	Ara	GlcN	Gal	Glc	Man	Rib	GalA	GlcA
EPS/EM-1	-1 (1.0)	-1 (100)	74.75	0.70	0.67	1.08	0.53	14.27	78.62	0.00	0.00	2.77	1.36
EPS/EM-2	1 (2.0)	-1 (100)	117.01	0.46	0.83	1.06	0.75	12.96	79.03	0.00	0.00	3.14	1.77
EPS/EM-3	-1 (1.0)	1 (300)	228.34	2.48	2.75	3.65	2.49	13.00	56.15	5.52	2.01	6.87	5.09
EPS/EM-4	1 (2.0)	1 (300)	68.70	0.00	0.00	0.90	1.29	15.32	79.58	0.00	0.00	2.91	0.00
EPS/EM-5	−1.41 (0.8)	0 (200)	93.04	0.45	0.07	0.81	0.30	14.17	79.87	0.00	0.00	3.41	0.92
EPS/EM-6	1.41 (2.2)	0 (200)	133.47	0.34	0.46	3.01	0.87	13.46	76.46	0.00	0.00	3.88	1.51
EPS/EM-7	0 (1.5)	−1.41 (59)	90.52	0.89	1.18	1.50	1.34	14.03	76.58	0.00	0.00	3.02	1.47
EPS/EM-8	0 (1.5)	1.41 (341)	178.64	0.00	0.39	0.52	0.43	16.45	72.72	0.00	0.00	3.44	6.03
EPS/EM-9	0 (1.5)	0 (200)	134.85	0.59	1.25	1.01	0.76	13.65	77.07	0.00	0.00	4.01	1.66
EPS/EM-10	0 (1.5)	0 (200)	140.02	0.78	1.12	1.37	0.99	14.06	77.61	0.00	0.00	2.85	1.22
EPS/EM-11	0 (1.5)	0 (200)	145.14	0.24	0.49	1.78	0.86	13.45	76.70	0.00	0.00	4.58	1.90

Fuc (fucose), Rha (rhamnose), Ara (arabinose), GlcN (glucosamine), Gal (galactose), Glc (glucose), Man (mannose), Rib (ribose), GalA (galacturonic acid), GlcA (glucuronic acid).

2.3.1. General conditions and sample preparation

Rheological measurements were conducted using an MCR92 modular compact rheometer (Anton Paar, Graz, Austria) featuring a cone-plate geometry (angle 2°, diameter 35 mm, 0.145 mm gap). A Peltier system maintained the temperature at 25 °C, except during temperature variation assessments. To minimize solvent evaporation during measurements, the sample perimeter was sealed with a layer of low-viscosity paraffin oil (Carl Roth, Karlsruhe, Germany), which exhibits a dynamic viscosity ranging from 0.025 to 0.080 Pa·s at 20 °C. For all analyses, the freeze-dried polymer was dispersed in pre-weighed deionized water and stirred until fully dissolved to obtain the desired concentrations.

2.3.2. Steady-state flow behavior

To assess the impact of production conditions, the steady-state flow behavior (0.01 s^{-1} to 1000 s^{-1}) of a 1.0 wt% solution of each EPS sample from the experimental design was analyzed. Subsequently, the biopolymer produced under the condition that yielded the highest EPS concentration (EPS/EM-4, 7.40 g L^{-1}; data for all runs ranged from 3.00 to 7.40 g L^{-1}) was selected for a more detailed rheological characterization. This detailed investigation evaluated the effect of polymer concentration (0.01 to 3.0 wt%) and pH (3 to 9) on the flow curves. The experimental data were fitted using the Carreau-Yasuda model (Eq. (1)).

$$\eta(\dot{\gamma}) = \eta_\infty + \frac{(\eta_0 - \eta_\infty)}{[1 + (\lambda\dot{\gamma})^a]^{\frac{n-1}{a}}} \quad (1)$$

where η is the apparent viscosity (Pa·s), $\dot{\gamma}$ is the shear rate (s^{-1}), λ is a time constant (s), η_0 (Pa·s) is the zero-shear rate viscosity, η_∞ is the viscosity of the second Newtonian plateau (Pa·s), n is the power-law index, and a is the Yasuda parameter. The model was simplified for fitting by disregarding the η_∞ term, as the second Newtonian plateau was not reached under the experimental conditions.

The goodness-of-fit for the Carreau-Yasuda model was evaluated based on the coefficient of determination (R^2) and the mean relative error (MRE).

2.3.3. Viscoelastic properties

The viscoelastic properties (G' and G") were determined using a standard protocol. First, amplitude sweep tests were performed over a strain range of 0.01% to 100% (at 1 Hz) to determine the linear viscoelastic region (LVER). Subsequently, frequency sweep tests were conducted from 0.01 to 10 Hz at a constant strain of 0.1% (within the LVER).

This methodology was applied to (i) evaluate a 1.0 wt% solution of each of the samples from the CCRD and (ii) conduct a detailed characterization of EPS/EM-4, investigating the influence of polymer concentration (0.01 to 3.0 wt%) and pH (3 to 9).

2.3.4. Effect of temperature

The effect of temperature on the rheological properties was investigated on a 1.0 wt% solution prepared from the EPS/EM-4 through both isothermal and continuous measurements. To further characterize the material's behavior, isothermal tests, including steady-state flow curves (shear rate 0.01 to 1000 s^{-1}) and oscillatory frequency sweeps (frequency 0.01 to 10 Hz, strain 0.1%), were performed at discrete temperatures of 0, 5, 15, 25, 35, 45, 55, 65, 75, 85, and 95 °C. For the continuous tests, the sample was subjected to a steady-state temperature ramp by heating from 0 to 95 °C and subsequently cooling to 0 °C at a rate of 6 °C min^{-1}, all under a constant shear rate of 10 s^{-1}. An oscillatory temperature sweep was also performed by heating the sample to 95 °C at 6 °C min^{-1}, holding for 10 min, and then cooling to 0 °C, with measurements taken at a constant strain of 0.1% and frequency of 1 Hz.

2.3.5. Time-dependent behavior

The thixotropy and structural recovery of the material were investigated on a 1.0 wt% solution of EPS/EM-4. A thixotropic loop test was performed by increasing the shear rate from 0.01 s^{-1} to 1000 s^{-1}, holding it at the maximum rate for 60 s, and then decreasing it back to 0.01 s^{-1}. Structural recovery was assessed using a three-step test: (1) 120 s under LVE conditions, (2) 60 s at a shear rate of 1000 s^{-1}, and (3) 200 s again in the LVE region, all at a frequency of 1 Hz.

2.4. Statistical analysis

When applicable, the results are shown as the mean values ± standard deviations. The analysis of the Central Composite Rotatable Design (CCRD), Analysis of Variance (ANOVA), and Pearson correlation analysis were performed using the Statistica 12 software program (StatSoft Inc., USA). The fitting of experimental data to the rheological model was performed using OriginPro 2025b software (OriginLab Corporation, Northampton, MA, USA).

3. Results

3.1. Carbohydrate analysis

The analysis of the monosaccharide composition (Table 1) reveals that the biopolymers produced by *E. meliloti* SEMIA 135 are heteropolysaccharides with a complex and variable composition, predominantly composed of glucose (56.15–79.87%) and galactose (12.96–16.45%). This profile is consistent with other EPS from *E. meliloti* and members of the Rhizobiaceae family [23,24]. Additionally, the presence of uronic acids (galacturonic and glucuronic acids), at total

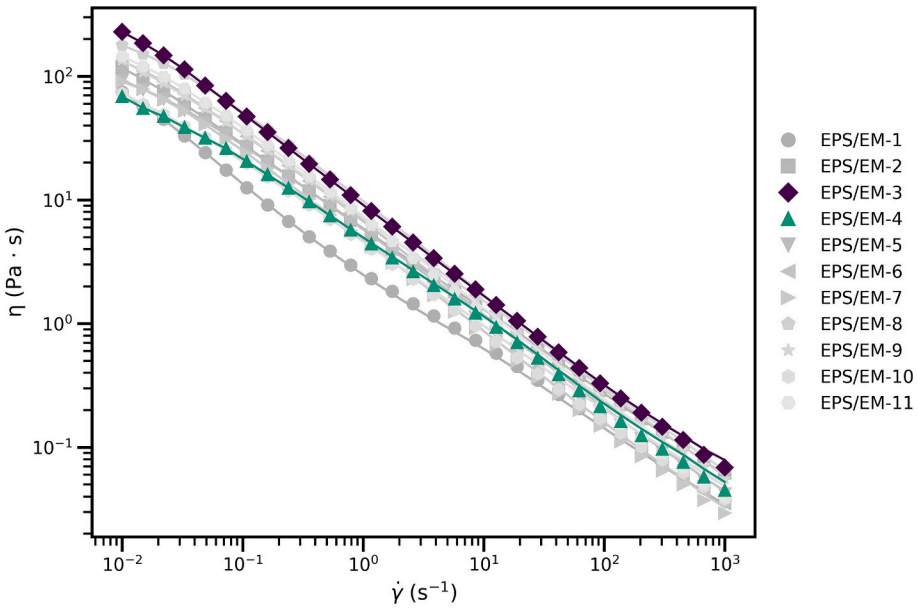

Fig. 1. Apparent viscosity (η) of EPS solutions (1.0 wt%, pH 7.0 and 25 °C) as a function of shear rate ($\dot{\gamma}$). EPS were obtained under different assay conditions using Central Composite Rotatable Design (CCRD). The lines correspond to the curves fitted to Carreau-Yasuda model.

contents varying from 2.91 to 11.96%, confers an anionic character to the polymers, a typical feature of bacterial EPS and a key determinant of their physicochemical and biological properties [12,13].

Beyond these major components, Table 1 shows a diverse array of minor sugars (e.g., fucose, rhamnose, arabinose, mannose, and ribose) at lower concentrations. It is important to emphasize that the purification process employed effectively removes free monosaccharides and small oligosaccharides originating from soybean molasses. Therefore, the detection of these sugars after acid hydrolysis confirms that they are integral components of the bacterial exopolysaccharide structure rather than residual contaminants from the culture medium. While this complex profile might suggest an improbable repeating unit structure if all monomers were part of the main backbone, this composition is, in fact, a well-documented characteristic of Rhizobiaceae heteropolysaccharides [25]. The literature indicates that these EPSs are typically composed of a high-glucose/galactose backbone that is then decorated with various minor neutral sugars, such as ribose, fucose, rhamnose, mannose, and uronic acids, which are suggested to exist as terminal groups or in short side chains [25–28]. The presence of these minor monomers is thus consistent with the complex diversity in EPS chemical structure, including branching patterns and non-carbohydrate substituents widely reported for rhizobial EPS [23,29,30].

The most significant outcome of this analysis is the strong influence of production conditions on the EPS monosaccharide composition. Systematic variation in aeration and agitation, as defined by the CCRD, not only altered the proportions of the major sugars but also affected the incorporation of minor sugars, demonstrating the sensitivity of the microorganism's biosynthetic pathways to oxygen availability and hydrodynamic stress. Other studies have also reported that cultivation parameters such as carbon sources [31] and pH [32], as well as aeration and agitation rates, can alter the composition of EPS in different microorganisms. Xu and Yun [27], for instance, found that varying aeration rates significantly affected the chemical composition and molecular weight of different exopolysaccharide fractions produced by *Paecilomyces tenuipes*. Corroborating this observation, Assis et al. [29], investigating xanthan gum production from crude glycerin, noted that aeration and agitation significantly influenced the biopolymer's chemical composition. In their results, low agitation rates increased the concentrations of glucose and pyruvic acid in the xanthan chain, while increased agitation contributed to a higher concentration of mannose. Additionally, decreasing the aeration rate led to higher concentrations of glucose and mannose in the polymer chain.

This sensitivity to cultivation conditions is particularly evident in EPS/EM-3, which displayed the most diverse composition, with elevated levels of minor sugars and unique detection of mannose and ribose, suggesting a pronounced metabolic shift induced by the combined effects of low aeration and high agitation. According to Rehm [33], such stress conditions can activate alternative enzymatic routes that alter the intracellular pool of nucleoside diphosphate sugars, the direct precursors for polysaccharide biosynthesis. Specifically, hydrodynamic and oxygen-limitation stress may regulate enzymes such as UDP-glucose dehydrogenase, which catalyzes the conversion of UDP-glucose to UDP-glucuronic acid [31,34]. An increased intracellular pool of this precursor would directly favor its incorporation into the growing polysaccharide chain, leading to the observed structural modifications and higher charge density. Furthermore, the physical shear stress generated by high agitation rates can act as an environmental trigger [14]. In response to shear-induced cellular stress, bacteria often upregulate the production of highly charged, mucoid EPS as a protective boundary mechanism to maintain cell membrane integrity and microbial fitness [7,33]. Conversely, conditions combining high aeration and high agitation (e.g., EPS/EM-4: 2.0 vvm, 300 rpm) provide an oxygen-rich environment that prioritizes central carbon metabolism and rapid cellular respiration. This metabolic state often diverts energy away from complex secondary biosynthetic pathways, thereby favoring the secretion of simpler, glucose-rich polymers [19].

3.2. Rheological properties

3.2.1. Effect of cultivation conditions

The steady-state flow behavior of the EPS solutions obtained from the CCRD is presented in Fig. 1. All samples displayed strong shear-thinning (pseudoplastic) behavior, with apparent viscosity decreasing linearly on a log–log scale over several orders of magnitude of shear rate. This response, typical of structured polymer solutions, is consistent with reports for other microbial biopolymers [8,22,35–39]. Although the qualitative flow behavior was consistent across all samples, the absolute viscosity varied markedly depending on cultivation conditions, with the solution from EPS/EM-3 showing the highest viscosity at low shear rates and EPS/EM-4 showing the lowest.

Table 2
Carreau-Yasuda model parameters estimated for Central Composite Rotatable Design (CCRD) EPS solutions (1.0 wt%, pH 7.0 and 25 °C).

EPS solution	η_0 (Pa·s)	λ (s)	a (−)	n (−)	R^2	MRE (%)
EPS/EM-1	122 ± 4.08	157 ± 0.98	2.00 ± 0.00	0.209 ± 0.009	0.999	19.9
EPS/EM-2	224 ± 1.86	193 ± 1.75	1.27 ± 0.13	0.305 ± 0.006	0.999	7.6
EPS/EM-3	328 ± 1.29	121 ± 4.52	1.83 ± 0.14	0.249 ± 0.005	0.999	6.3
EPS/EM-4	95.7 ± 1.74	210 ± 7.29	0.43 ± 0.17	0.265 ± 0.093	0.999	7.2
EPS/EM-5	193 ± 1.01	104 ± 3.55	0.74 ± 0.05	0.238 ± 0.013	0.999	6.4
EPS/EM-6	266 ± 1.63	138 ± 5.36	0.93 ± 0.07	0.250 ± 0.010	0.999	9.8
EPS/EM-7	120 ± 2.93	82.6 ± 1.56	1.46 ± 0.08	0.268 ± 0.007	0.999	5.7
EPS/EM-8	326 ± 1.35	79.7 ± 2.86	0.81 ± 0.04	0.195 ± 0.014	0.999	3.5
EPS/EM-9	264 ± 2.94	207 ± 4.96	0.44 ± 0.08	0.215 ± 0.037	0.999	11.4
EPS/EM-10	143 ± 1.38	137 ± 4.54	0.39 ± 0.07	0.212 ± 0.045	0.999	6.9
EPS/EM-11	297 ± 1.40	122 ± 3.12	0.84 ± 0.05	0.226 ± 0.010	0.999	2.2

η = apparent viscosity (Pa·s), $\dot{\gamma}$ = shear rate (s^{-1}), λ = time constant (s), η_0 = zero-shear rate viscosity (Pa·s), η_∞ = viscosity of the second Newtonian plateau (Pa·s), n = power-law index, a = Yasuda parameter, R^2 = coefficient of determination, MRE = mean relative error.
The experiments were conducted according to a central composite rotational design (CCRD), combining different levels of aeration (0.8–2.2 vvm) and agitation (59–341 rpm): EPS/EM-1 (1.0 vvm; 100 rpm), EPS/EM-2 (2.0 vvm; 100 rpm), EPS/EM-3 (1.0 vvm; 300 rpm), EPS/EM-4 (2.0 vvm; 300 rpm), EPS/EM-5 (0.8 vvm; 200 rpm), EPS/EM-6 (2.2 vvm; 200 rpm), EPS/EM-7 (1.5 vvm; 59 rpm), EPS/EM-8 (1.5 vvm; 341 rpm), and EPS/EM-9 to 11 (1.5 vvm; 200 rpm).

The experimental flow curves were fitted using the Carreau-Yasuda model (Eq. 1). Although the flow behavior in the measured range (0.01 to 1000 s^{-1}) was dominated by shear-thinning, fitting the data to the Carreau-Yasuda model allows for the estimation of the zero-shear viscosity (η_0), a critical parameter representing the material's structure at rest. Unlike the Power Law model, which predicts infinite viscosity at zero shear rate [38], the Carreau-Yasuda model provides a physically realistic description of polymer solutions by assuming a finite viscosity limit at low deformation rates. The robust fit ($R^2 > 0.999$) confirms the model's suitability for these EPS solutions, where chain entanglement leads to pronounced pseudoplasticity [38].

To quantify these effects, the model parameters were obtained for each sample (Table 2), where all regressions yielded high determination coefficients ($R^2 \geq 0.999$) and low mean relative errors (MRE < 20%), confirming the robustness of the model. The results indicate that samples synthesized under conditions favoring high viscosity (e.g., EPS/EM-3 and 8) exhibit larger η_0 and relaxation time constant (λ) values; physically, a higher η_0 reflects a denser network with stronger intermolecular interactions and maximal resistance to flow before structural disruption, while λ serves as a critical indicator of the dynamic response, representing the characteristic time required for polymer chains to disentangle and reorient. In this context, the significantly higher values observed for EPS/EM-3 suggest that its chains are highly entangled or possess higher molecular weights typical of polymers with more extended chains [40], thereby requiring longer timescales to unravel compared to lower viscosity variants.

Physically, η_0 reflects the structural integrity of the polymer network in a quasi-equilibrium state, representing the maximal resistance to flow before the macromolecular structure is disrupted by shear forces. A higher η_0 implies a denser network with stronger intermolecular interactions. Furthermore, λ serves as a critical indicator of the material's dynamic response. It represents the characteristic time required for the polymer chains to disentangle and reorient in the direction of flow. In this context, the significantly higher λ values observed for EPS/EM-3 suggest that its chains are highly entangled or possess higher molecular weights, requiring longer timescales to unravel compared to the lower viscosity variants.

To further elucidate how culture parameters affect the polymer network, oscillatory frequency sweeps were performed (Fig. 2). Across all samples, the mechanical spectra exhibited $G' > G''$ over the entire frequency range, indicating dominant elastic behavior characteristic of weak gels or highly structured polymer solutions [8]. This elastic dominance suggests that even at low frequencies (long timescales), the EPS forms a percolated network of entangled and associated chains. Similar viscoelastic profiles have been reported for EPS produced by *Alteromonas macleodii* Mo 169 [8] and *Rhizobium radiobacter* S10 [41].

Notably, the nature of the viscoelastic response was modulated by the production parameters. In several samples (EPS/EM-2, 4, 7, 10, and 11), G' and G'' were close at low frequencies and diverged with increasing frequency, implying that polymer chains can disentangle and rearrange over long timescales, leading to partial energy dissipation [41]. In contrast, EPS/EM-3 presented well-separated, nearly parallel G' and G'' curves, with $G' \gg G''$ even at low frequencies, a signature of a more solid-like, stable network [8,41]. Overall, this confirms that production conditions modulated both the magnitude of viscosity and the nature of the viscoelastic response, with conditions such as those of EPS/EM-4 yielding a viscous, entangled liquid, whereas EPS/EM-3 generated a more persistent weak gel.

To statistically quantify the influence of aeration and agitation on these observed rheological differences and understand their predictive relationship, Response Surface Methodology (RSM) was employed. The apparent viscosity at a shear rate of 0.01 s^{-1} was selected as the key response variable. As shown in Table 1, this viscosity varied markedly among the CCRD experiments, ranging from 68.7 Pa·s (EPS/EM-4) to 228.3 Pa·s (EPS/EM-3).

The experimental data were fitted to a second-order polynomial regression model (Eq. 2). The ANOVA results (Table 3) confirmed that the model was statistically significant ($F = 12.33 > F_{critical} = 4.46$, $p < 0.05$) and provided a satisfactory fit ($r = 0.87$), demonstrating that viscosity variation was attributable to the studied factors rather than random error.

$$Viscosity\ (Pa\ s) = 127.679 + 28,776 \bullet X_2 - 50,475 \bullet X_1X_2 \quad (2)$$

Analysis of the model and contour plot (Fig. 3) revealed that the interaction between aeration (X_1) and agitation (X_2) was the most influential term, exhibiting a strong negative coefficient (−50.48). This indicates an antagonistic relationship: maximum viscosity (> 225 Pa·s) occurred under low aeration (~1.0 vvm) and high agitation (> 300 rpm), whereas high aeration combined with high agitation produced the lowest viscosities (< 75 Pa·s).

This interaction likely reflects distinct metabolic responses of *E. meliloti* to culture stress. Although the molecular weight distribution for each of the 11 samples was not determined in this study, a limitation that prevents quantifying the specific contribution of chain length to the observed viscosity variations, our previous work under optimized conditions reported a high molecular weight of approximately 9.27×10^7

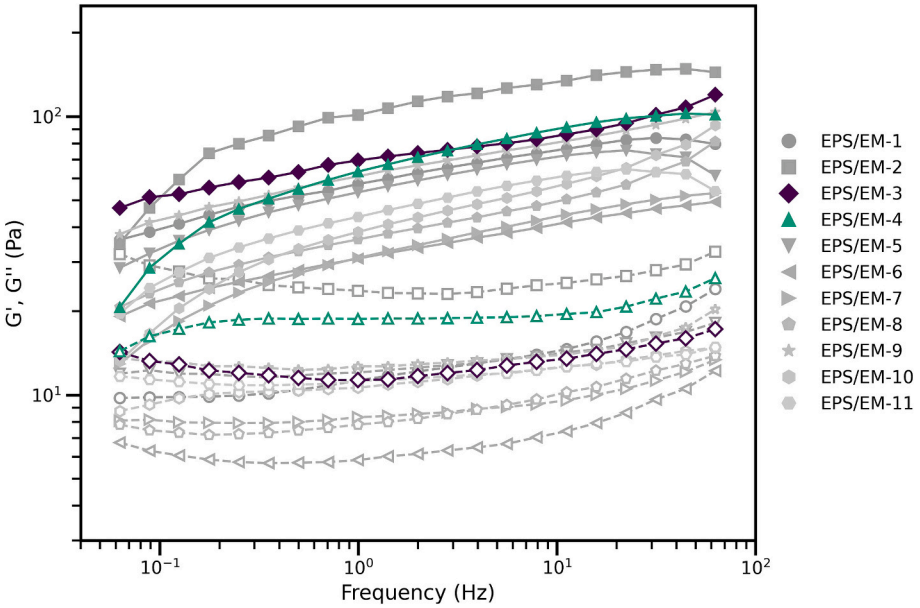

Fig. 2. Angular frequency dependencies of storage (G', filled symbols) and loss (G", open symbols) moduli for the aqueous solutions of *E. meliloti* SEMIA 135 EPS at Central Composite Rotatable Design (CCRD): EPS/EM-1 (1.0 vvm; 100 rpm), EPS/EM-2 (2.0 vvm; 100 rpm), EPS/EM-3 (1.0 vvm; 300 rpm), EPS/EM-4 (2.0 vvm; 300 rpm), EPS/EM-5 (0.8 vvm; 200 rpm), EPS/EM-6 (2.2 vvm; 200 rpm), EPS/EM-7 (1.5 vvm; 59 rpm), EPS/EM-8 (1.5 vvm; 341 rpm), and EPS/EM-9 to 11 (1.5 vvm; 200 rpm).

Table 3
ANOVA of the Central Composite Design (CCRD) for EPS apparent viscosity ($p = 0.05$).

Variation source	DF	SQ	MQ	F_{cal}	$F_{critical}$	r
Regression	2	16,795.37	8397.68	12.33	4.46	0.87
Residual	8	5449.78	681.22			
Total	10	22,245.15				

SQ, sum of squares; DF, degrees of freedom; MQ, mean squares.

Da for this EPS [22]. While variations in chain length likely contribute to the rheological differences, the significant changes in viscosity observed here are strongly supported by the modulation of the polymer's chemical composition, particularly its charge density.

To clarify the structural basis of viscosity changes, a Pearson correlation analysis was performed linking monosaccharide composition to apparent viscosity (Fig. 4). Strong positive correlations were found for galacturonic ($p = 0.0006$) and glucuronic acids ($p = 0.0007$), confirming that the anionic character of the polymer is a major determinant of viscosity. Uronic acids, through their carboxyl groups, which are

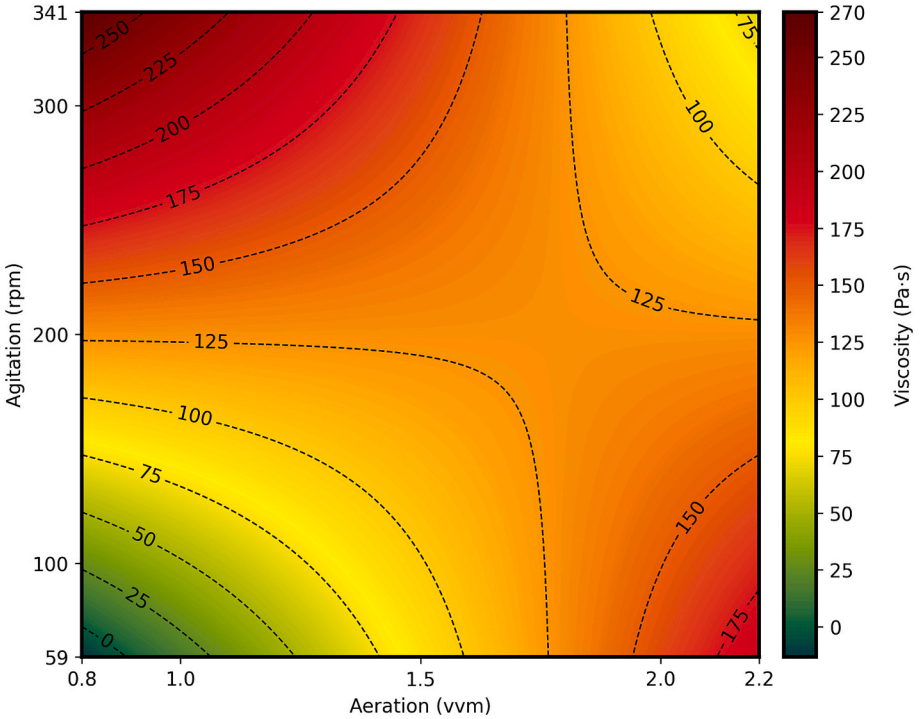

Fig. 3. Contour plot of the Central Composite Rotatable Design (CCRD) for EPS apparent viscosity ($p = 0.05$).

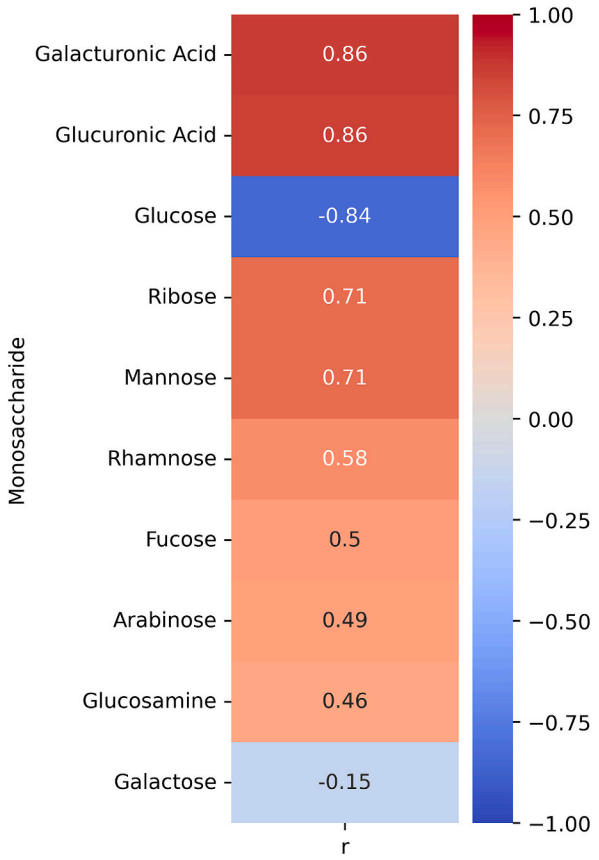

Fig. 4. Pearson correlation heatmap illustrating the relationship between the relative content of each monosaccharide and the apparent viscosity of the EPS solutions. The *p*-values for the correlations are: galacturonic acid ($p = 0.0006$), glucuronic acid ($p = 0.0007$), glucose ($p = 0.0012$), ribose ($p = 0.0138$), mannose (p = 0.0138), rhamnose ($p = 0.0589$), fucose ($p = 0.1163$), arabinose ($p = 0.1287$), glucosamine ($p = 0.1572$), and galactose (p = 0.6567). Correlations with $p < 0.05$ were considered statistically significant.

deprotonated at neutral pH, impart negative charges that cause intramolecular and intermolecular electrostatic repulsion, expanding the polymer coils and increasing hydrodynamic volume and resistance to flow [42,43].

Conversely, glucose content displayed a significant negative correlation with viscosity ($p = 0.0012$). This result should not be interpreted as glucose intrinsically impairing viscosity but rather as a compositional trade-off inherent to heteropolysaccharides. Since the monosaccharide composition is relative, a higher proportional content of neutral glucose monomers necessarily implies a reduced fraction of anionic species. Consequently, this dilution of charge density diminishes the intramolecular electrostatic repulsion that drives chain expansion [42,43], leading to a more compact hydrodynamic volume and, ultimately, lower solution viscosity. This agrees with the profile of EPS/EM-3, which exhibited both the lowest glucose fraction and the highest content of uronic acids and viscosity. These results indicate that specific cultivation regimes act as metabolic triggers shifting EPS biosynthesis toward uronic acid enrichment, which directly enhances viscosity. In contrast, conditions combining high aeration and agitation favor simpler, glucose-rich polymers with lower viscosity. Interestingly, galactose ($p = 0.6567$), the second most abundant monosaccharide, showed no significant correlation with viscosity.

This phenomenon finds parallels in other biopolymer studies. For example, Assis et al. [29], when optimizing xanthan gum production, also identified a strong link between cultivation parameters and rheological properties. In their study, agitation and aeration exhibited a quadratic effect on viscosity, with an optimal point (1.05 vvm and ~ 500 rpm) maximizing apparent viscosity. Deviating from this optimum point, whether through excessively high or low agitation, resulted in lower viscosity. The study established a direct correlation between viscosity, molecular weight, and pyruvic acid content. It was found that distinct conditions impaired the biosynthetic pathway responsible for adding the pyruvic acid groups. Without these anionic groups, the chain, even if long, did not expand and did not generate the expected high viscosity. This reinforces the conclusion that hydrodynamic and oxygen transfer conditions are critical tools for modulating the monosaccharide composition and charged group content, determining the final EPS rheology.

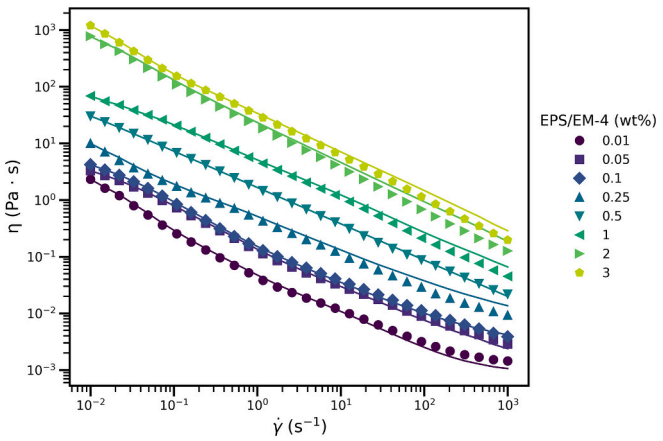

Fig. 5. Apparent viscosity (η) of EPS/EM-4 (2.0 vvm, 300 rpm) solutions (pH 7 and 25 °C) as a function of shear rate ($\dot{\gamma}$) at different concentrations. The lines correspond to the curves fitted to Carreau-Yasuda model.

Table 4
Carreau-Yasuda model parameters estimated for EPS/EM-4 (2.0 vvm, 300 rpm) solutions (pH 7 and 25 °C) at different concentrations.

EPS/EM (wt%)	η_0 (Pa·s)	λ (s)	a (−)	n (−)	R^2	MRE (%)
0.01	5.48 ± 0.09	255 ± 0.27	1.99 ± 0.20	0.050 ± 0.029	0.999	14.0
0.05	5.87 ± 0.37	111 ± 3.92	1.06 ± 0.09	0.183 ± 0.015	0.999	13.2
0.10	6.06 ± 0.67	99.5 ± 4.14	2.00 ± 0.00	0.215 ± 0.010	0.999	12.2
0.25	15.8 ± 1.94	288 ± 5.70	0.41 ± 0.11	0.380 ± 0.037	0.999	5.9
0.50	83.7 ± 3.96	421 ± 2.79	1.27 ± 0.54	0.348 ± 0.011	0.999	1.7
1.00	95.7 ± 1.74	210 ± 7.29	0.43 ± 0.17	0.265 ± 0.093	0.999	7.2
2.00	947 ± 1.80	287 ± 3.01	1.97 ± 0.17	0.167 ± 0.016	0.999	15.0
3.00	1263 ± 1.51	105 ± 1.43	1.40 ± 0.58	0.120 ± 0.013	0.999	15.2

η = apparent viscosity (Pa·s), $\dot{\gamma}$ = shear rate (s^{-1}), λ = time constant (s), η_0 = zero-shear rate viscosity (Pa·s), η_∞ = viscosity of the second Newtonian plateau (Pa·s), n = power-law index, a = Yasuda parameter, R^2 = coefficient of determination, MRE = mean relative error.

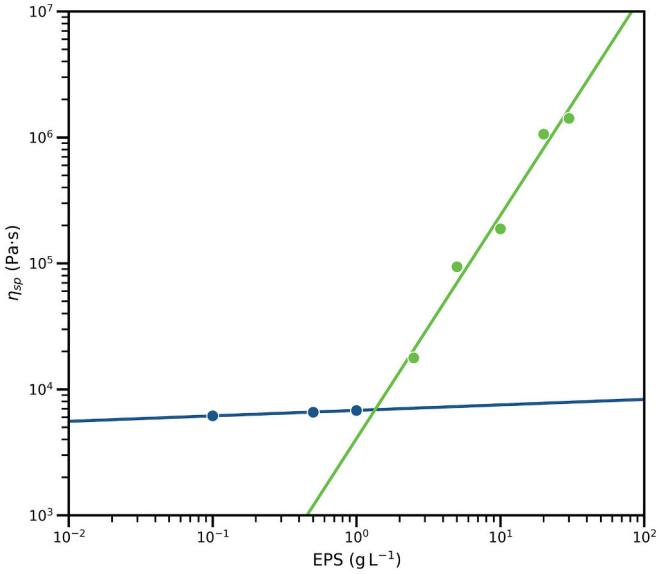

Fig. 6. Concentration dependence of the zero-shear specific viscosity (η_{sp}) of EPS/EM-4 (2.0 vvm, 300 rpm).

3.2.2. *Effect of concentration*

Fig. 5 illustrates the effect of EPS/EM-4 concentration on flow behavior. As the concentration increased, the viscosity rose sharply, and the flow curves shifted upward. At a shear rate of 0.1 s^{-1}, the apparent viscosity increased by more than two orders of magnitude, from 5 Pa·s to over 1000 Pa·s. This trend is characteristic of polymer solutions, resulting from intensified intermolecular interactions and entanglements as chain proximity increases, demonstrating that EPS is a highly effective thickening agent [8,44].

Table 4 presents the Carreau-Yasuda model parameters for this sample as a function of concentration. The data highlight that concentration is a critical factor, with the zero-shear viscosity (η_0) increasing over 200-fold as the concentration rose from 0.01 to 3.00 wt%. This was accompanied by a decrease in the power-law index (n), indicating that more concentrated solutions also exhibit more pronounced shear-thinning behavior.

All solutions exhibited pronounced shear-thinning behavior, and the viscosity was high at low shear rates and decreased markedly as shear increased, reflecting chain disentanglement and alignment in the flow direction. This combination of high zero-shear viscosity and strong pseudoplasticity is a desirable property for hydrocolloids, contributing to controllable texture and processability [45].

The plot in Fig. 6 illustrates the dependence of the zero-shear specific viscosity (η_{sp}) on the EPS concentration. Two distinct regions with varying slopes can be clearly identified, providing insight into the polymer's hydrodynamic volume and chain-chain interactions. At low concentrations, η_{sp} scales linearly with concentration. In this dilute regime, the polymer chains are hydrodynamically isolated coils; the viscosity increase is driven solely by the individual contributions of discrete polymer molecules and their interaction with the solvent, without significant intermolecular overlap [46,47].

However, a critical transition occurs at the overlap concentration (c* = 1,35 g L^{-1}). Above this point, the dependence of η_{sp} on concentration becomes much stronger, exhibiting a steep power-law slope. This transition marks the onset of the semi-dilute entangled regime, where the polymer coils begin to overlap and interpenetrate [8]. In this state, the motion of individual chains is topologically constrained by neighboring chains (entanglements), leading to an increase in flow resistance. The sharp rise in specific viscosity indicates that the EPS effectively builds a continuous transient network even at relatively low concentrations, a key feature for its application as an efficient thickening agent [8].

The viscoelastic properties further confirmed the structural evolution with concentration (Fig. 7). Both storage (G′) and loss (G″) moduli increased with frequency, indicating viscoelastic behavior typical of polymer solutions. At low concentrations (0.01–0.1 wt%), G″ exceeded G′, revealing that viscous behavior predominated due to limited molecular interactions. As the concentration rose (0.25–1 wt%), both moduli increased substantially, and G′ surpassed G″, indicating a transition toward elastic or solid-like behavior caused by the formation of an entangled molecular network [8,48].

At the highest concentrations (2–3 wt%), G′ dominated G″ across all frequencies, and both moduli became nearly frequency-independent. This plateau behavior signifies the formation of a stronger, percolated gel network where molecular mobility is highly restricted. Overall, these results demonstrate that the *E. meliloti* EPS transitions from a viscous solution at dilute regimes to a weak gel at higher concentrations, driven

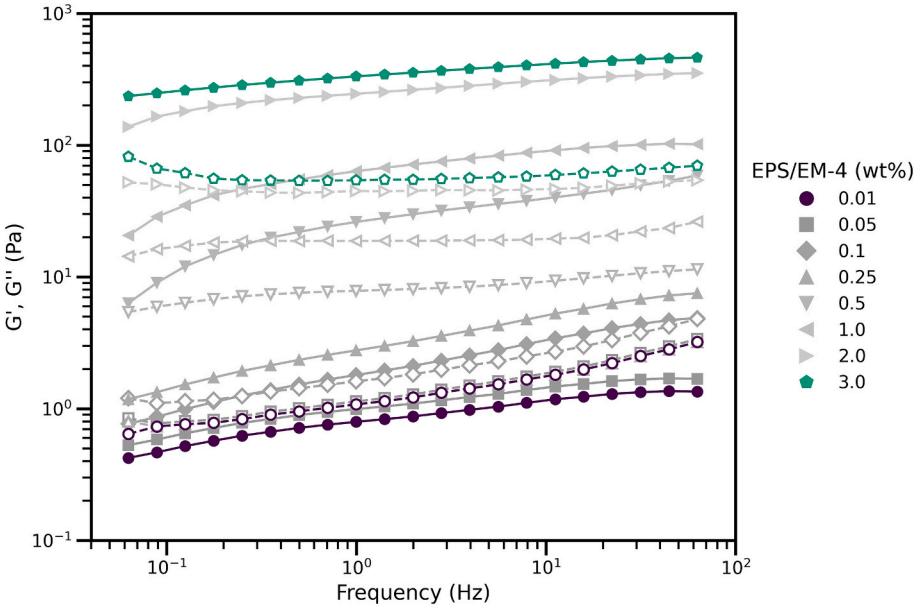

Fig. 7. Angular frequency dependencies of storage (G', filled symbols) and loss (G", open symbols) moduli for the aqueous solutions of EPS/EM-4 (2.0 vvm, 300 rpm) at different concentrations (wt%): 0.01, 0.05, 0.1, 0.25, 0.5, 1.0, 2.0, and 3.0.

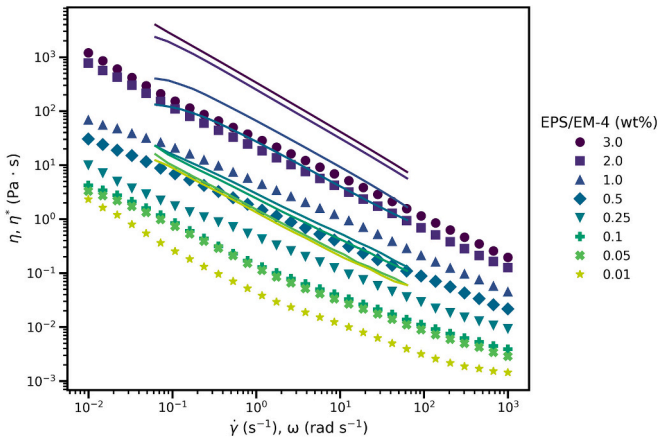

Fig. 8. Cox-Merz plot for the aqueous solutions of EPS/EM-4 (2.0 vvm, 300 rpm) at different concentrations. Apparent viscosity (η, symbols) and complex viscosity (η*, lines) as a function of shear rate (γ̇) and angular frequency (ω), respectively.

by progressive intermolecular association and chain entanglement. According to Fan et al. [48], in strong gels, the elastic modulus (G′) typically exceeds the viscous modulus (G″) by at least one order of magnitude, indicating predominantly elastic behavior.

Variations in the rheological properties of polysaccharides, such as their ability to form gels, are attributed to differences in their structural characteristics, including monosaccharide composition, glycosidic bond types, charge density, and molecular mass distribution [49]. This explains why some polymers exhibit gel-like behavior, while others do not. For instance, gel formation has been reported for polysaccharides from *Alteromonas macleodii* Mo 169 (>0.4 wt%) [8,49], *Rhizobium leguminosarum* bv. *viciae* VF39 (>4.0 wt%) [50] and *Rhizobium radiobacter* S10 (>0.75 wt%) [40].

Fig. 8 presents the Cox-Merz plot, which compares the steady-shear apparent viscosity (η) as a function of shear rate (γ̇) with the complex viscosity (η*) as a function of angular frequency (ω). This empirical relationship is a powerful tool for probing the structural nature of polymer solutions, as it reveals how the material responds to different types of deformation [51].

In all cases, the complex viscosity is systematically and significantly higher than the steady-shear apparent viscosity. This failure of the Cox-Merz rule is the classic and unambiguous signature of a highly structured fluid, such as an associative polymer solution or a weak physical gel [8,51]. This behavior is explained by the fundamental difference between the two measurement techniques. The oscillatory test, which measures η*, is a small-amplitude, nondestructive probe [52]. It measures the resistance of the intact, three-dimensional, at-rest network structure. In contrast, the steady-shear test, which measures η, is a continuous, large-deformation, and destructive experiment [53]. It forces the material to flow, which breaks down the associative network. The resulting viscosity measurement therefore reflects the resistance of the "broken-down" state, which is much lower. Several polysaccharides have been shown to diverge from this rule, including xanthan [54], *Aeromonas* gum [55], and hyaluronic acid [56].

The observation that this deviation persists even at high concentrations (e.g., 3 wt%) is a significant finding. This indicates that the system does not behave as a simple entangled polymer solution, which would typically be expected to obey the rule. Instead, the data strongly suggest that the EPS forms an associative network. This behavior is likely governed by specific, noncovalent intermolecular interactions, such as hydrogen bonding or ionic associations, rather than simple physical entanglements [54]. Alternatively, such deviations are frequently attributed to structural heterogeneities inherent to complex biopolymers, including the presence of microgel particles, hyperbranched structures, or stiff chain conformations that resist small-amplitude oscillatory strains but align and yield under continuous shear flow [51,54]. While direct spectroscopic and light-scattering evidence is needed to fully uncouple these structural contributions, the macroscopic rheological signature provides compelling evidence for a structured, gel-like fluid. This hypothesis fully supports the previous observations of gel-like behavior (G' > G") across a wide range of conditions, a signature characteristic of high-performance rheology modifiers such as xanthan gum and essential for applications requiring the suspension of solids, such as in foods, cosmetics, or coatings [54].

3.2.3. *Effect of pH*

The influence of pH on the steady-shear and viscoelastic properties of the EPS solution (EPS/EM-4, at 1 wt%) was examined across the pH 3–9 range. Regardless of pH, all solutions maintained strong pseudoplastic

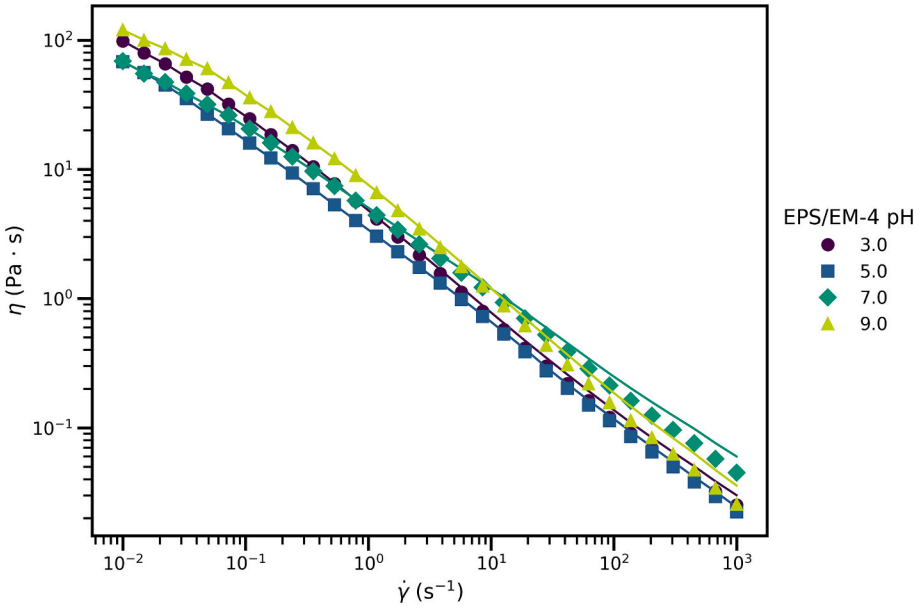

Fig. 9. Apparent viscosity (η) of EPS/EM-4 solutions (2.0 vvm, 300 rpm; 1.0 wt%) as a function of shear rate ($\dot{\gamma}$) for different pH values. The lines correspond to the curves fitted to Carreau-Yasuda model.

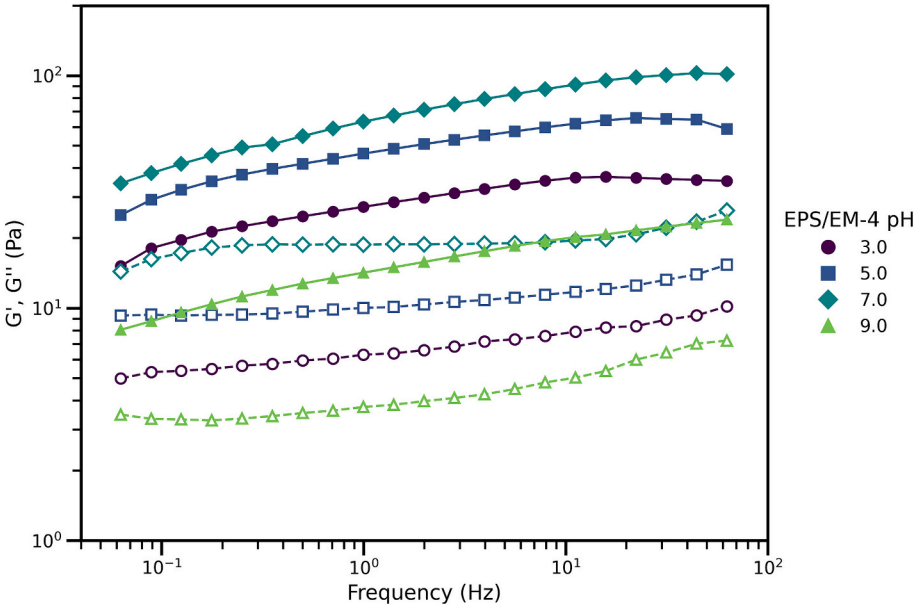

Fig. 10. Angular frequency dependencies of storage (G', filled symbols) and loss (G", open symbols) moduli for the aqueous solutions of EPS/EM-4 (2.0 vvm, 300 rpm) at different pH values: 3.0, 5.0, 7.0, and 9.0.

Table 5
Carreau-Yasuda model parameters estimated for EPS/EM-4 (2.0 vvm, 300 rpm) solutions (1 wt% and 25 °C) at different pH values.

pH	η_0 (Pa·s)	λ (s)	a (−)	n (−)	R^2	MRE (%)
3	137 ± 2.74	88.8 ± 6.16	0.34 ± 0.08	0.123 ± 0.011	0.999	5.3
5	94.6 ± 3.68	125 ± 5.43	1.93 ± 0.16	0.314 ± 0.004	0.999	13.5
7	95.7 ± 1.74	210 ± 7.29	0.43 ± 0.17	0.265 ± 0.093	0.999	7.2
9	167 ± 1.19	32.1 ± 1.48	0.45 ± 0.13	0.157 ± 0.008	0.999	6.4

η = apparent viscosity (Pa·s), $\dot{\gamma}$ = shear rate (s^{-1}), λ = time constant (s), η_0 = zero-shear rate viscosity (Pa·s), η_∞ = viscosity of the second Newtonian plateau (Pa·s), n = power-law index, a = Yasuda parameter, R^2 = coefficient of determination, MRE = mean relative error.

behavior (Fig. 9), and G′ remained consistently higher than G″ (Fig. 10), confirming the presence of a stable weak-gel network with dominant elastic character. The estimated rheological parameters are summarized in Table 5.

The EPS exhibited a clear pH dependence, with a minimum viscosity at near-neutral pH and elevated viscosity at acidic and alkaline extremes. Under alkaline conditions, the viscosity increased significantly. This behavior is characteristic of anionic polyelectrolytes. At this pH, the carboxyl groups are fully deprotonated, maximizing the net negative charge density along the polymer backbone [22]. This amplifies intramolecular electrostatic repulsion, forcing the chains to adopt a more expanded conformation with a larger hydrodynamic volume, which consequently leads to higher viscosity and gel strength. This observed increase in viscosity with pH aligns with the behavior reported for EPS produced by *Sphingomonas* sp. [57] and *Leuconostoc citreum*-BMS [37].

Conversely, at the acidic extreme, protonation of the chains occurs. This neutralizes the negative charge and reduces electrostatic repulsion. While chain contraction and lower viscosity would typically be expected, the observed increase suggests that hydrogen bonding between the partially neutralized chains becomes the dominant interaction mechanism [22]. This interaction favors the formation of a denser, more structured network, resulting in higher viscosity and elasticity. Variations in pH response are often attributed to differences in the composition and interactions of the specific components of each EPS [22].

3.2.4. *Effect of temperature*

The thermal dependence of the EPS rheological properties was investigated through steady-shear flow and dynamic temperature-sweep experiments. As shown in Fig. 11, the apparent viscosity decreased with increasing temperature, while the pseudoplastic character was preserved across all conditions. This behavior, common among biopolymer hydrocolloids, results from increased molecular mobility and disruption of temperature-sensitive intermolecular interactions such as hydrogen bonds [58]. The quantitative impact of temperature on the model parameters is detailed in Table 6. The data reveal a clear inverse relationship between η_0 and temperature, suggesting a loss of structural organization at thermal extremes.

A temperature ramp test (Fig. 12) confirmed this trend: viscosity declined gradually up to ~65 °C, followed by a sharp drop, indicating a thermally induced transition.

During cooling, the viscosity partially recovered but did not return to its initial value, showing clear thermal hysteresis. This irreversibility suggests that the heat-induced disassembly of the polymer network is not fully reversible within the experimental timeframe, likely due to incomplete reassociation of chains once disordered [59]. This type of behavior is characteristic of biopolymers that undergo thermally induced, irreversible conformational changes, such as gellan gum [60]. These findings demonstrate that EPS functions effectively as a thickening agent under ambient or refrigerated conditions but loses part of its structural organization after exposure to high temperatures, which is relevant for processes such as pasteurization and sterilization [61].

The viscoelastic response (Figs. 13–14) supported this conclusion. Frequency sweeps revealed a gradual transition from gel-like ($G' > G''$) to liquid-like ($G'' > G'$) behavior at high temperatures. However, it is important to note that the exact gel-sol transition is frequency-dependent. Based on the temperature-sweep test performed at a fixed frequency of 1 Hz (Fig. 14), a macroscopic gel-sol transition was identified at approximately 70 °C, where G′ and G″ intersected. Upon cooling, both moduli increased again but remained significantly below their initial values, confirming that the thermal disruption of the network was only partially reversible. To quantify this, a comparison of the initial and

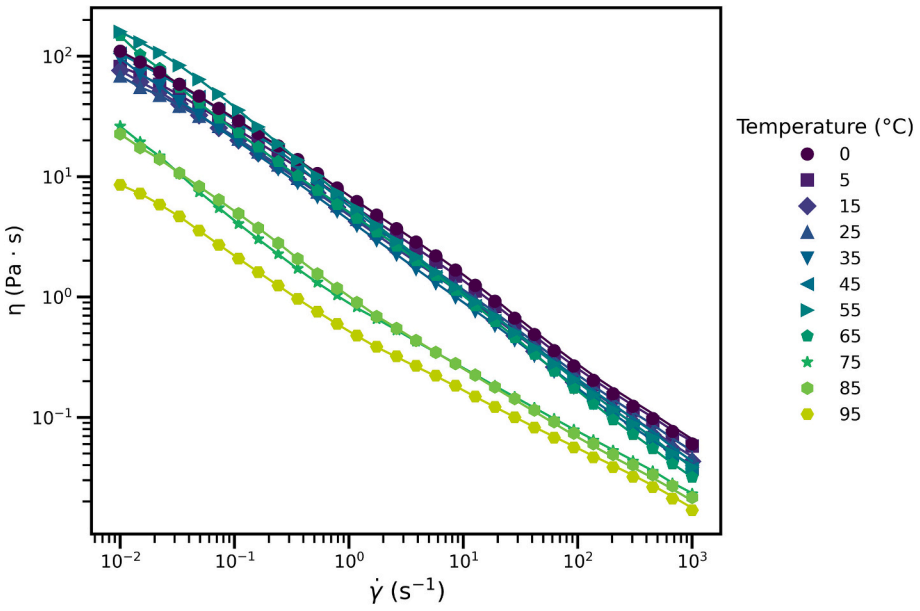

Fig. 11. Apparent viscosity (η) of EPS/EM-4 solutions (2.0 vvm, 300 rpm; 1.0 wt%) as a function of shear rate ($\dot{\gamma}$) for different temperatures. The lines correspond to the curves fitted to Carreau-Yasuda model.

Table 6
Carreau-Yasuda model parameters estimated for EPS/EM-4 (2.0 vvm, 300 rpm) solutions (1 wt% and pH 7) at different temperatures.

T (°C)	η_0 (Pa·s)	λ (s)	a (−)	n (−)	R^2	MRE (%)
0	471 ± 8.04	489 ± 7.27	0.59 ± 0.07	0.325 ± 0.011	0.999	7.3
5	141 ± 0.76	141 ± 0.72	1.05 ± 0.08	0.366 ± 0.007	0.999	13.8
15	106 ± 0.68	147 ± 1.74	0.30 ± 0.08	0.240 ± 0.053	0.999	4.2
25	95.7 ± 1.74	210 ± 0.73	0.43 ± 0.17	0.265 ± 0.093	0.999	7.2
35	173 ± 0.96	249 ± 2.09	1.89 ± 0.04	0.336 ± 0.005	0.999	9.9
45	140 ± 4.89	124 ± 1.07	2.00 ± 0.00	0.365 ± 0.011	0.999	8.2
55	312 ± 2.00	104 ± 3.67	0.91 ± 0.07	0.146 ± 0.018	0.999	10.7
65	222 ± 1.35	79.7 ± 2.86	0.81 ± 0.04	0.195 ± 0.014	0.999	14.7
75	40.3 ± 3.33	166 ± 1.68	2.62 ± 0.40	0.210 ± 0.014	0.999	15.7
85	33.9 ± 1.38	275 ± 4.54	0.39 ± 0.07	0.212 ± 0.045	0.999	9.7
95	9.83 ± 0.41	95.7 ± 4.70	2.95 ± 0.05	0.341 ± 0.007	0.999	12.6

η = apparent viscosity (Pa·s), $\dot{\gamma}$ = shear rate (s^{-1}), λ = time constant (s), η_0 = zero-shear rate viscosity (Pa·s), η_∞ = viscosity of the second Newtonian plateau (Pa·s), n = power-law index, a = Yasuda parameter, R^2 = coefficient of determination, MRE = mean relative error.

final states reveals that upon cooling back to 0 °C, the storage modulus (G′) recovered approximately 20.6% of its initial magnitude. The large gap between the heating and cooling curves indicates that the reassociation kinetics are slow, producing a weaker and less ordered structure after cooling. This kinetically dependent renaturation, where the cooling path differs from the heating path, is a well-documented phenomenon for other network-forming biopolymers [59,60].

3.2.5. Thixotropy

The thixotropic behavior and structural recovery of the EPS solution

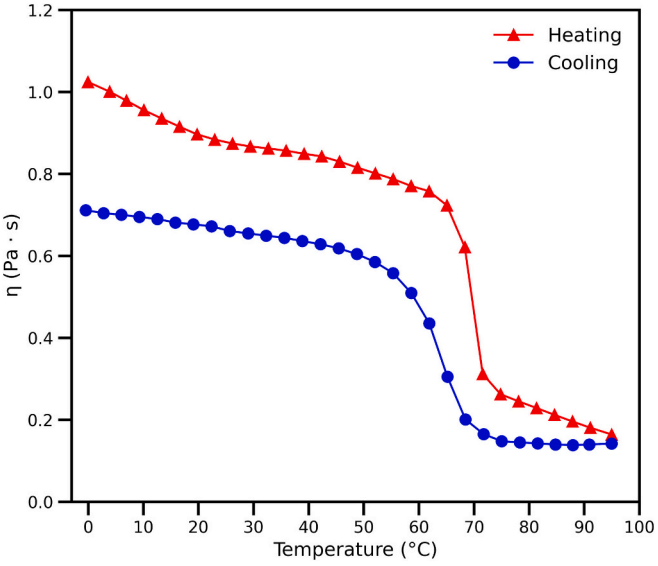

Fig. 12. Temperature sweep for the aqueous solution of EPS/EM-4 (2.0 vvm, 300 rpm; 1.0 wt%) at a fixed shear rate of 10 s^{-1} during heating from 0 to 95 °C (red) and subsequent cooling from 95 to 0 °C (blue). (For interpretation of the references to colour in this figure legend, the reader is referred to the web version of this article.)

were evaluated to assess its response under high shear, an important property for many practical applications. Fig. 15 shows the results of a three-stage oscillatory time test monitoring G′ and G″ before and after a high-shear event.

In the first stage (0–120 s), the solution exhibited a stable weak-gel structure, with G′ constant and much higher than G″. During the second stage, a 60 s high-shear period (1000 s^{-1}) was applied, followed by recovery at rest (180–380 s). Immediately after shear cessation, G′ dropped sharply, confirming network disruption, but progressively increased over time as the structure rebuilt itself. This recovery was fast yet incomplete: most gel strength returned quickly, although G′ did not fully reach its initial value within the experimental window. Such partial, time-dependent recovery is characteristic of thixotropic materials

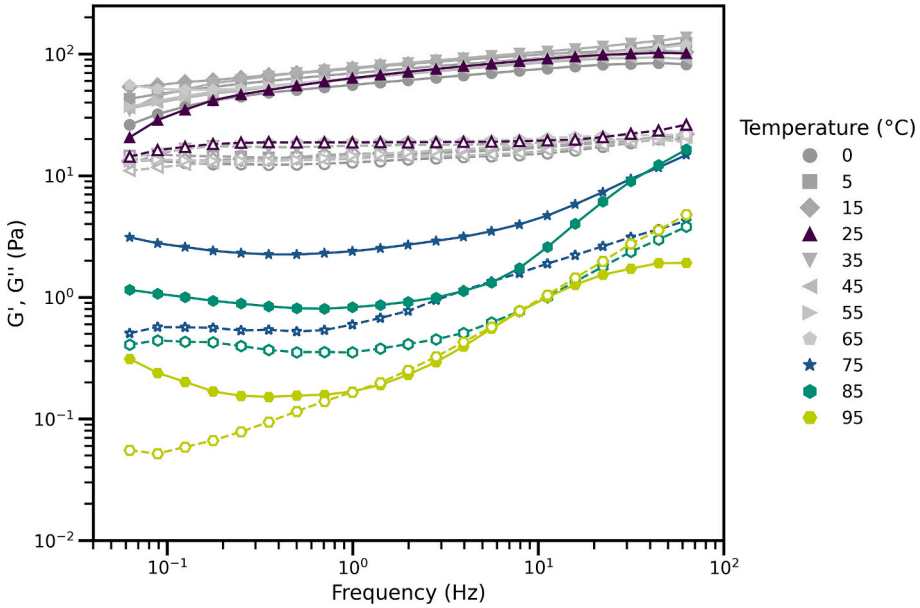

Fig. 13. Angular frequency dependencies of storage (G', filled symbols) and loss (G", open symbols) moduli for the aqueous solutions of EPS/EM-4 (2.0 vvm, 300 rpm) at different temperatures (°C): 0, 5, 15, 25, 35, 45, 55, 65, 75, 85, and 95.

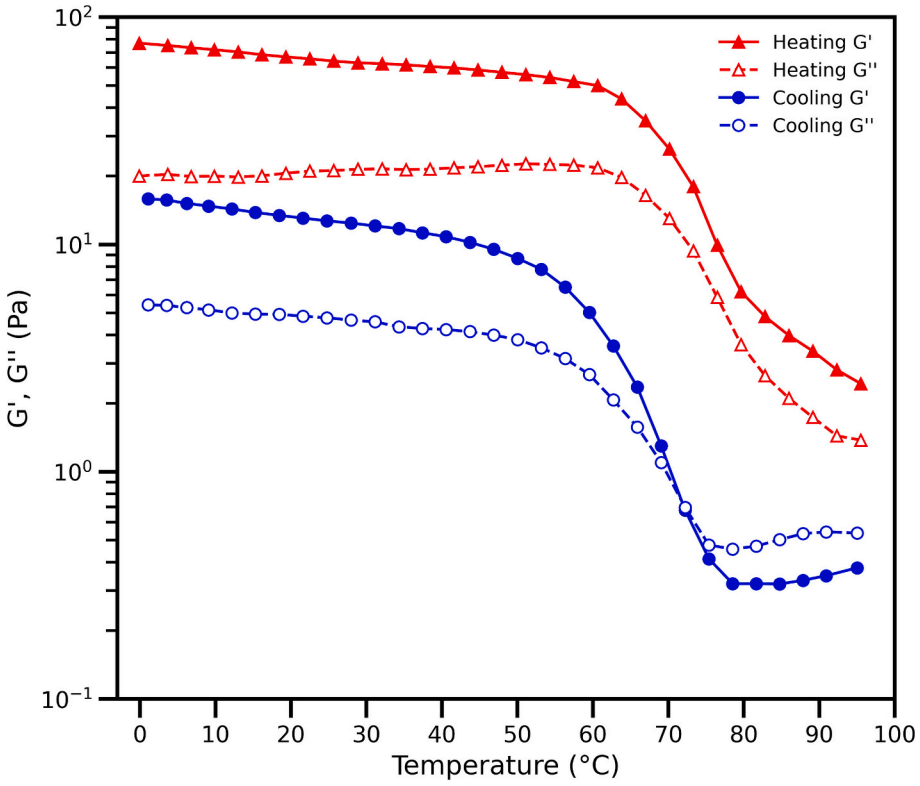

Fig. 14. Temperature dependence of storage (G') and loss (G") moduli for the aqueous solution of EPS/EM-4 (2.0 vvm, 300 rpm) during heating from 0 to 95 °C (red) and cooling from 95 to 0 °C (blue). (For interpretation of the references to colour in this figure legend, the reader is referred to the web version of this article.)

[62], in which physical associations reform rapidly while long-range organization is slower to re-establish [63].

To complement this test, a thixotropic loop was performed by increasing and then decreasing the shear rate (Fig. 16). The coincident upward and downward flow curves showed no hysteresis, indicating that structural breakdown and recovery occur on timescales shorter than the measurement itself [62].

Although the two tests may seem contradictory, they capture distinct aspects of the same phenomenon. The loop test reflects fast, short-term dynamics, while the step-shear test reveals slower, long-term network reformation. This concept of thixotropy involving multiple, distinct timescales for structural recovery is a well-established principle for complex fluids [62]. Together, they show that the EPS behaves as a structured fluid capable of near-instantaneous realignment under shear but requires longer times to fully rebuild its weak-gel network once the stress is removed.

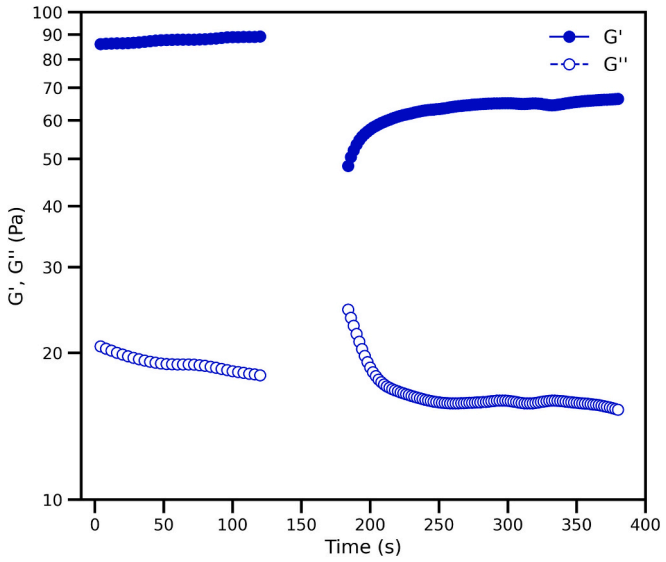

Fig. 15. Thixotropic behavior of EPS/EM-4 solution (2.0 vvm, 300 rpm; 1.0 wt %): Storage (G') and loss (G") moduli before and after exposure to high shear conditions (1000 s^{-1} between 120 and 180 s).

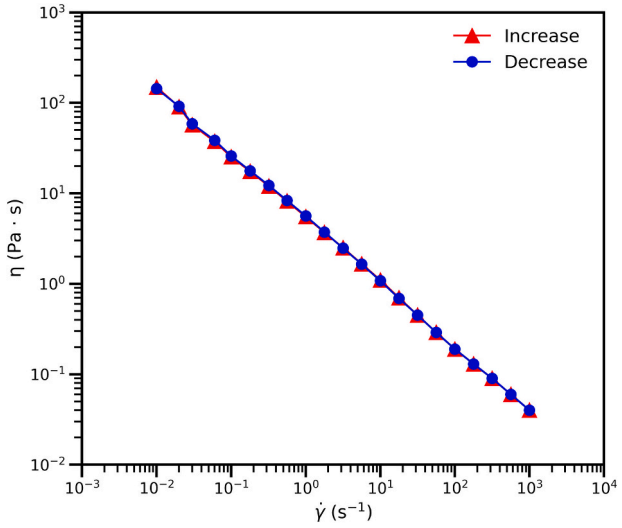

Fig. 16. Thixotropic behavior of EPS/EM-4 solution (2.0 vvm, 300 rpm; 1.0 wt %): Effect of high shear stress on the apparent viscosity (η), with shear rate ($\dot{\gamma}$) increasing from 0.01 to 1000 s^{-1}, kept at 1000 s^{-1} for 60 s, and decreased from 1000 to 0.01 s^{-1}.

These characteristics are highly desirable for industrial applications that involve mixing, pumping, or dispensing. The combination of rapid viscosity recovery and resistance to structural collapse ensures good processability while maintaining stability at rest. Such behavior is advantageous for products requiring controlled flow and texture, such as food gels, coatings, and cosmetic formulations [63], where the material must flow easily under shear but quickly regain its structure afterward.

4. Conclusions

This study successfully validates a rational bioprocessing framework for customizing the functionality of bacterial exopolysaccharides. We demonstrated that bioreactor hydrodynamics are not merely operational variables but decisive metabolic triggers that dictate the chemical architecture of the *Ensifer meliloti* SEMIA 135 EPS. By strategically manipulating aeration and agitation, it was possible to steer the biosynthesis toward uronic acid-rich polymers, thereby amplifying the charge density and driving a threefold increase in apparent viscosity.

Critically, the rheological analysis revealed that this EPS functions as a sophisticated associative thickener rather than a simple viscosifier. Its distinct weak-gel character, violation of the Cox-Merz rule, and rapid thixotropic recovery confirm its potential to compete with high-performance commercial hydrocolloids in applications requiring stability at rest and flow under shear, such as in injectable formulations or structured foods.

Ultimately, this work shifts the paradigm from trial-and-error cultivation to predictive materials design. This proves that the "bio-factory" approach allows for the in-situ fine-tuning of polymer properties without the need for complex postproduction chemical modifications or genetic engineering. This tunability establishes *E. meliloti* SEMIA 135 EPS as a versatile, sustainable candidate for the next generation of smart functional biomaterials.

Future research will focus on determination of the EPS molecular weight distribution, chain conformation analysis, and transcriptomic profiling to fully elucidate the metabolic and structural mechanisms underlying this tunability.

CRediT authorship contribution statement

Rui dos Santos Ferreira Filho: Writing – original draft, Visualization, Methodology, Investigation, Funding acquisition, Formal analysis, Conceptualization. **Filomena Freitas:** Writing – review & editing, Supervision, Resources, Methodology. **Janaína Fernandes de Medeiros Burkert:** Writing – review & editing, Supervision, Resources, Methodology, Funding acquisition, Conceptualization. **Carlos André Veiga Burkert:** Writing – review & editing, Supervision, Resources, Project administration, Methodology, Funding acquisition, Conceptualization.

Funding

This work was supported by FAPERGS (Foundation Research Support in the State of Rio Grande do Sul) (Grant Number 24/2551–0001776-3) and the Coordination for the Improvement of Higher Education Personnel (CAPES) (Finance Code 001). This work was also financed by national funds from FCT/MCTES - Fundação para a Ciência e a Tecnologia, I.P., Ministério da Ciência, Tecnologia e Ensino Superior, Portugal, in the scope of the projects UIDP/04378/2020 and UIDB/04378/2020 of the Research Unit on Applied Molecular Biosciences – UCIBIO, and project LA/P/0140/202019 of the Associate Laboratory Institute for Health and Bioeconomy – i4HB.

Declaration of competing interest

The authors declare that they have no known competing financial interests or personal relationships that could have appeared to influence the work reported in this paper.

Acknowledgements

The authors would like to thank the Coordination for the Improvement of Higher Education Personnel - Brazil (CAPES) (Finance Code 001) and the Foundation Research Support in Rio Grande do Sul state (FAPERGS) (Grant Number 24/2551-0001776-3) that funded this study.

Data availability

Data will be made available on request.

References

[1] S. Pirsa, K. Hafezi, Hydrocolloids: structure, preparation method, and application in food industry, Food Chem. 399 (2023) 133967, https://doi.org/10.1016/J.FOODCHEM.2022.133967.

[2] Y. Gao, R. Liu, H. Liang, Food hydrocolloids: structure, properties, and applications, Foods 13 (2024) 1077, https://doi.org/10.3390/foods13071077.

[3] N. Nguyen, A.S. Dulai, S. Adnan, Z. Khan, R.K. Sivamani, Narrative review of the use of hydrocolloids in dermatology: applications and benefits, J. Clin. Med. 14 (2025) 1345, https://doi.org/10.3390/jcm14041345.

[4] M. Mohd Nadzir, R.W. Nurhayati, F.N. Idris, M.H. Nguyen, Biomedical applications of bacterial exopolysaccharides: a review, Polymers (Basel). 13 (2021) 530, https://doi.org/10.3390/polym13040530.

[5] H.-T. Nguyen, T.-T. Pham, P.-T. Nguyen, H. Le-Buanec, H.N. Rabetafika, H. L. Razafindralambo, Advances in microbial exopolysaccharides: present and future applications, Biomolecules 14 (2024) 1162, https://doi.org/10.3390/biom14091162.

[6] M. Sharma, N. Tellili, I. Kacem, T. Rouissi, Microbial biopolymers: from production to environmental applications—a review, Appl. Sci. 14 (2024) 5081, https://doi.org/10.3390/app14125081.

[7] F. Freitas, C.A.V. Torres, M.A.M. Reis, Engineering aspects of microbial exopolysaccharide production, Bioresour. Technol. 245 (2017) 1674–1683, https://doi.org/10.1016/J.BIORTECH.2017.05.092.

[8] P. Concórdio-Reis, S.S. Ferreira, V.D. Alves, X. Moppert, J. Guézennec, M. A. Coimbra, M.A.M. Reis, F. Freitas, Rheological characterization of the exopolysaccharide produced by *Alteromonas macleodii* Mo 169, Int. J. Biol. Macromol. 227 (2023) 619–629, https://doi.org/10.1016/J.IJBIOMAC.2022.12.117.

[9] P. Li, Y. Bai, Y. Yang, M. Li, Structural characterization of exopolysaccharide produced by *Streptococcus thermophilus* and rheology of mixed protein-polysaccharide systems, Food Biosci. 55 (2023) 102961, https://doi.org/10.1016/J.FBIO.2023.102961.

[10] D. Li, J. Li, F. Zhao, G. Wang, Q. Qin, Y. Hao, The influence of fermentation condition on production and molecular mass of EPS produced by *Streptococcus thermophilus* 05-34 in milk-based medium, Food Chem. 197 (2016) 367–372, https://doi.org/10.1016/J.FOODCHEM.2015.10.129.

[11] F. Li, X. Hu, X. Sun, H. Li, J. Lu, Y. Li, M. Bao, Effect of fermentation pH on the structure, rheological properties, and antioxidant activities of exopolysaccharides produced by *Alteromonas australica* QD, Glycoconj. J. 39 (2022) 773–787, https://doi.org/10.1007/s10719-022-10087-3.

[12] A. Shukla, M. Tangney, Bacterial exopolysaccharides and live biotherapeutics: orchestrating immune modulation and therapeutic potential in the gut microbiome era, Biomed. Pharmacother. 191 (2025) 118510, https://doi.org/10.1016/J.BIOPHA.2025.118510.

[13] C. Laroche, Exopolysaccharides from microalgae and cyanobacteria: diversity of strains, production strategies, and applications, Mar. Drugs 20 (2022) 336, https://doi.org/10.3390/md20050336.

[14] J.-J. Zhong, Recent advances in bioreactor engineering, Korean J. Chem. Eng. 27 (2010) 1035–1041, https://doi.org/10.1007/s11814-010-0277-5.

[15] H.-U. Peters, H. Herbst, P.G.M. Hesselink, H. Lünsdorf, A. Schumpe, W.-D. Deckwer, The influence of agitation rate on xanthan production by *Xanthomonas campestris*, Biotechnol. Bioeng. 34 (1989) 1393–1397, https://doi.org/10.1002/bit.260341108.

[16] A.T. Granja, A. Popescu, A.R. Marques, I. Sá-Correia, A.M. Fialho, Biochemical characterization and phylogenetic analysis of UDP-glucose dehydrogenase from the gellan gum producer *Sphingomonas elodea* ATCC 31461, Appl. Microbiol. Biotechnol. 76 (2007) 1319–1327, https://doi.org/10.1007/s00253-007-1112-8.

[17] A.R. Rashidi, N.I.W. Azelee, D.N.A. Zaidel, L.F. Chuah, A. Bokhari, H.A. El Enshasy, D.J. Dailin, Unleashing the potential of xanthan: a comprehensive exploration of biosynthesis, production, and diverse applications, Bioprocess Biosyst. Eng. 46 (2023) 771–787, https://doi.org/10.1007/s00449-023-02870-9.

[18] D. de J. Assis, L.V. Brandão, L.A. de Sousa Costa, T.V.B. Figueiredo, L.S. Sousa, F. F. Padilha, J.I. Druzian, A study of the effects of aeration and agitation on the properties and production of xanthan gum from crude glycerin derived from biodiesel using the response surface methodology, Appl. Biochem. Biotechnol. 172 (2014) 2769–2785, https://doi.org/10.1007/s12010-014-0723-7.

[19] C.P. Xu, J.W. Yun, Influence of aeration on the production and the quality of the exopolysaccharides from *Paecilomyces tenuipes* C240 in a stirred-tank fermenter, Enzym. Microb. Technol. 35 (2004) 33–39, https://doi.org/10.1016/J.ENZMICTEC.2004.03.012.

[20] K. Parmar, D. Patel, B. Iyer, Adhesive potential of *Priestia aryabhattai* KAG-18 exopolysaccharide: surface bonding, material properties, and finite element modeling, J. Polym. Environ. 33 (2025) 5109–5129, https://doi.org/10.1007/s10924-025-03694-2.

[21] F. Horkay, J.F. Douglas, S.R. Raghavan, Rheological properties of cartilage glycosaminoglycans and proteoglycans, Macromolecules 54 (2021) 2316–2324, https://doi.org/10.1021/acs.macromol.0c02709.

[22] R.S. Ferreira Filho, J.F.M. Burkert, C.A.V. Burkert, From shake flasks to a bench-scale bioreactor: scaling up exopolysaccharide production in fed-batch cultivation of *Ensifer meliloti* SEMIA 135, J. Chem. Technol. Biotechnol. 100 (2025) 1818–1830, https://doi.org/10.1002/jctb.7916.

[23] A. Skorupska, M. Janczarek, M. Marczak, A. Mazur, J. Król, Rhizobial exopolysaccharides: genetic control and symbiotic functions, Microb. Cell Factories 5 (2006) 7, https://doi.org/10.1186/1475-2859-5-7.

[24] M. Janczarek, Environmental signals and regulatory pathways that influence exopolysaccharide production in rhizobia, Int. J. Mol. Sci. 12 (2011) 7898–7933, https://doi.org/10.3390/ijms12117898.

[25] T.C.L. Castellane, A.M.M.B. Otoboni, E.G. de M. Lemos, Characterization of exopolysaccharides produced by rhizobia species, Rev. Bras. Cienc. Solo 39 (2015) 1566–1575, https://doi.org/10.1590/01000683RBCS20150084.

[26] Y. Kaci, A. Heyraud, M. Barakat, T. Heulin, Isolation and identification of an EPS-producing *Rhizobium* strain from arid soil (Algeria): characterization of its EPS and the effect of inoculation on wheat rhizosphere soil structure, Res. Microbiol. 156 (2005) 522–531, https://doi.org/10.1016/J.RESMIC.2005.01.012.

[27] R. Gharzouli, M.A. Carpéné, F. Couderc, A. Benguedouar, V. Poinsot, Relevance of fucose-rich extracellular polysaccharides produced by *Rhizobium sullae* strains nodulating *Hedysarum coronarium* L. legumes, Appl. Environ. Microbiol. 79 (2013) 1764–1776, https://doi.org/10.1128/AEM.02903-12.

[28] M. Marczak, A. Mazur, P. Koper, K. Żebracki, A. Skorupska, Synthesis of rhizobial exopolysaccharides and their importance for symbiosis with legume plants, Genes 8 (2017) 360, https://doi.org/10.3390/genes8120360.

[29] I.W. Sutherland, The biofilm matrix – an immobilized but dynamic microbial environment, Trends Microbiol. 9 (2001) 222–227, https://doi.org/10.1016/S0966-842X(01)02012-1.

[30] F. Donot, A. Fontana, J.C. Baccou, S. Schorr-Galindo, Microbial exopolysaccharides: Main examples of synthesis, excretion, genetics and extraction, Carbohydr. Polym. 87 (2012) 951–962, https://doi.org/10.1016/J.CARBPOL.2011.08.083.

[31] A. Angelov, A. Georgieva, M. Petkova, E. Bartkiene, J.M. Rocha, M. Ognyanov, V. Gotcheva, On the molecular selection of exopolysaccharide-producing lactic acid bacteria from indigenous fermented plant-based foods and further fine chemical characterization, Foods 12 (2023) 3346, https://doi.org/10.3390/foods12183346.

[32] Y. Ju, K. Shan, W. Liu, C. Xi, Y. Zhang, W. Wang, C. Wang, R. Cao, W. Zhu, H. Wang, Y. Zhao, L. Hao, Effect of different initial fermentation pH on exopolysaccharides produced by *Pseudoalteromonas agarivorans* Hao 2018 and identification of key genes involved in exopolysaccharide synthesis via transcriptome analysis, Mar. Drugs 20 (2022) 89, https://doi.org/10.3390/md20020089.

[33] B.H.A. Rehm, Bacterial polymers: biosynthesis, modifications and applications, Nat. Rev. Microbiol. 8 (2010) 578–592, https://doi.org/10.1038/nrmicro2354.

[34] Y. Bontemps, B. Vuillermoz, F. Antonicelli, C. Perreau, J.-L. Danan, F.-X. Maquart, Y. Wegrowski, Specific protein-1 is a universal regulator of UDP-glucose dehydrogenase expression: its positive involvement in transforming growth factor-β signaling and inhibition in hypoxia, J. Biol. Chem. 278 (2003) 21566–21575, https://doi.org/10.1074/jbc.M209366200.

[35] C.A.V. Torres, A.R.V. Ferreira, F. Freitas, M.A.M. Reis, I. Coelhoso, I. Sousa, V. D. Alves, Rheological studies of the fucose-rich exopolysaccharide FucoPol, Int. J. Biol. Macromol. 79 (2015) 611–617, https://doi.org/10.1016/J.IJBIOMAC.2015.05.029.

[36] Q. Meng, Q. Wang, L. Chen, J. Li, L. Fan, Z. Gu, G. Shi, Z. Ding, Rheological properties and thickening effect of high molecular weight exopolysaccharide and intracellular polysaccharide from *Schizophyllum commune*, Food Hydrocoll. 144 (2023) 108920, https://doi.org/10.1016/J.FOODHYD.2023.108920.

[37] Y. Abid, S. Azabou, C. Blecker, A. Gharsallaoui, M.M. Corsaro, S. Besbes, H. Attia, Rheological and emulsifying properties of an exopolysaccharide produced by potential probiotic *Leuconostoc citreum*-BMS strain, Carbohydr. Polym. 256 (2021) 117523, https://doi.org/10.1016/J.CARBPOL.2020.117523.

[38] H. Huang, Y. Wen, Z. Li, B. Wang, S. Li, Characterization and rheological properties of a new exopolysaccharide overproduced by *Rhizobium* sp. L01, Polymers (Basel). 17 (2025) 592, https://doi.org/10.3390/polym17050592.

[39] A. Huber, M. Koller, P. Wintersteller, A critical review of the microbial exopolysaccharide xanthan, Chem. Biochem. Eng. Q. 39 (2025) 65–87, https://doi.org/10.15255/CABEQ.2024.2348.

[40] R.A. Mohamed Yunus, D. Parisi, Scaling laws in polysaccharide rheology: comparative analysis of water and ionic liquid systems, Biomacromolecules 25 (2024) 6883–6898, https://doi.org/10.1021/acs.biomac.4c01125.

[41] F. Zhou, Z. Wu, C. Chen, J. Han, L. Ai, B. Guo, Exopolysaccharides produced by *Rhizobium radiobacter* S10 in whey and their rheological properties, Food Hydrocoll. 36 (2014) 362–368, https://doi.org/10.1016/J.FOODHYD.2013.08.016.

[42] B.L. Tardy, B.D. Mattos, C.G. Otoni, M. Beaumont, J. Majoinen, T. Kämäräinen, O. J. Rojas, Deconstruction and reassembly of renewable polymers and biocolloids into next generation structured materials, Chem. Rev. 121 (2021) 14088–14188, https://doi.org/10.1021/acs.chemrev.0c01333.

[43] K. Arab, B. Ghanbarzadeh, S. Karimi, B. Ebrahimi, M. Hosseini, Gelling and rheological properties of a polysaccharide extracted from *Ocimum album* L. seed, Int. J. Biol. Macromol. 246 (2023) 125603, https://doi.org/10.1016/J.IJBIOMAC.2023.125603.

[44] S. Ji, H. Li, G.H. Wang, T. Lu, W. Ma, J. Wang, H. Zhu, H. Xu, Rheological behaviors of a novel exopolysaccharide produced by *Sphingomonas* WG and the potential application in enhanced oil recovery, Int. J. Biol. Macromol. 162 (2020) 1816–1824, https://doi.org/10.1016/J.IJBIOMAC.2020.08.114.

[45] A. Yemenicioğlu, S. Farris, M. Turkyilmaz, S. Gulec, A review of current and future food applications of natural hydrocolloids, Int. J. Food Sci. Technol. 55 (2020) 1389–1406, https://doi.org/10.1111/ijfs.14363.

[46] W. Dridi, N. Bordenave, Influence of polysaccharide concentration on polyphenol-polysaccharide interactions, Carbohydr. Polym. 274 (2021) 118670, https://doi.org/10.1016/J.CARBPOL.2021.118670.

[47] S.A. Arvidson, B.T. Rinehart, F. Gadala-Maria, Concentration regimes of solutions of Levan polysaccharide from *Bacillus* sp, Carbohydr. Polym. 65 (2006) 144–149, https://doi.org/10.1016/J.CARBPOL.2005.12.039.
[48] Z. Fan, P. Cheng, P. Zhang, G. Zhang, J. Han, Rheological insight of polysaccharide/protein based hydrogels in recent food and biomedical fields: a review, Int. J. Biol. Macromol. 222 (2022) 1642–1664, https://doi.org/10.1016/j.ijbiomac.2022.10.082.
[49] P. Concórdio-Reis, V.D. Alves, X. Moppert, J. Guézennec, F. Freitas, M.A.M. Reis, Characterization and biotechnological potential of extracellular polysaccharides synthesized by *Alteromonas* strains isolated from French Polynesia marine environments, Mar. Drugs 19 (2021) 522, https://doi.org/10.3390/md19090522.
[50] S. Park, Y. Shin, S. Jung, Structural, rheological properties and antioxidant activities analysis of the exopolysaccharide produced by *Rhizobium leguminosarum* bv. *Viciae* VF39, Int. J. Biol. Macromol. 257 (2024) 128811, https://doi.org/10.1016/J.IJBIOMAC.2023.128811.
[51] V. Kontogiorgos, I. Margelou, N. Georgiadis, C. Ritzoulis, Rheological characterization of okra pectins, Food Hydrocoll. 29 (2012) 356–362, https://doi.org/10.1016/J.FOODHYD.2012.04.003.
[52] Q. Yuan, X. Lu, K.H. Khayat, D. Feys, C. Shi, Small amplitude oscillatory shear technique to evaluate structural build-up of cement paste, Mater. Struct. 50 (2017) 112, https://doi.org/10.1617/s11527-016-0978-2.
[53] J. Li, Y. Li, W. Xiao, J. Wang, B. Wang, Effect of shear history on solid–liquid transition of particulate gel fuels, Gels 9 (2023) 902, https://doi.org/10.3390/gels9110902.
[54] J.A. Carmona, A. Lucas, P. Ramírez, N. Calero, J. Muñoz, Nonlinear and linear viscoelastic properties of a novel type of xanthan gum with industrial applications, Rheol. Acta 54 (2015) 993–1001, https://doi.org/10.1007/s00397-015-0888-1.
[55] X. Xu, W. Liu, L. Zhang, Rheological behavior of *Aeromonas* gum in aqueous solutions, Food Hydrocoll. 20 (2006) 723–729, https://doi.org/10.1016/J.FOODHYD.2005.06.012.
[56] A.M.B. Pires, M.H.A. Santana, Rheological aspects of microbial hyaluronic acid, J. Appl. Polym. Sci. 122 (2011) 126–133, https://doi.org/10.1002/app.33976.
[57] S.-J. Miao, J. Zhou, G.-N. Qi, J.-F. Liu, S.-Z. Yang, H. Gang, B.-Z. Mu, Rheological properties of a new microbial exopolysaccharide produced by *Sphingomonas* sp. HS and its potential in enhanced oil recovery, Energy Fuel 36 (2022) 1792–1798, https://doi.org/10.1021/acs.energyfuels.1c02925.
[58] W. Cai, T. Hu, Q. Huang, A polysaccharide from *Lignosus rhinocerotis* sclerotia: self-healing properties and the effect of temperature on its rheological behavior, Carbohydr. Polym. 267 (2021) 118223, https://doi.org/10.1016/J.CARBPOL.2021.118223.
[59] S.M.A. Razavi, A. Alghooneh, F. Behrouzian, Thermo-rheology and thermodynamic analysis of binary biopolymer blend: a case study on sage seed gum-xanthan gum blends, Food Hydrocoll. 77 (2018) 307–321, https://doi.org/10.1016/J.FOODHYD.2017.10.007.
[60] E. Miyoshi, T. Takaya, K. Nishinari, Rheological and thermal studies of gel-sol transition in gellan gum aqueous solutions, Carbohydr. Polym. 30 (1996) 109–119, https://doi.org/10.1016/S0144-8617(96)00093-8.
[61] J. Liu, J. Bi, D.J. McClements, X. Liu, J. Yi, J. Lyu, M. Zhou, R. Verkerk, M. Dekker, X. Wu, D. Liu, Impacts of thermal and non-thermal processing on structure and functionality of pectin in fruit- and vegetable- based products: a review, Carbohydr. Polym. 250 (2020) 116890, https://doi.org/10.1016/J.CARBPOL.2020.116890.
[62] J. Mewis, N.J. Wagner, Thixotropy, Adv. Colloid Interf. Sci. 147–148 (2009) 214–227, https://doi.org/10.1016/J.CIS.2008.09.005.
[63] H.A. Barnes, Thixotropy—a review, J. Non-Newtonian Fluid Mech. 70 (1997) 1–33, https://doi.org/10.1016/S0377-0257(97)00004-9.